Journal of Inorganic Biochemistry 218 (2021) 111400

Contents lists available at ScienceDirect

Journal of Inorganic Biochemistry

journal homepage: www.elsevier.com/locate/jinorgbio

Mitochondrial targeted rhodium(III) complexes: Synthesis, characterized and antitumor mechanism investigation

Yan-Bo Peng [a], Can Tao [a], Cai-Ping Tan [b,*], Ping Zhao [a,*]

[a] School of Chemistry and Chemical Engineering, Guangdong Pharmaceutical University, Education Mega Centre, No. 280, Waihuandong Road, Guangzhou 510006, PR China

[b] MOE Key Laboratory of Bioinorganic and Synthetic Chemistry, School of Chemistry, Sun Yat-Sen University, Guangzhou 510275, PR China

ARTICLE INFO

Keywords:
Rhodium complexes
Mitochondrial
ROS
Apoptosis

ABSTRACT

Recently, rhodium complexes have received intensive attentions due to their tunable chemical and biological properties as well as attractive antitumor activity. In this work, two imidazole triphenylamino rhodium complexes [Rh(ppy)$_2$**L1**]PF6 **(Rh1)** and [Rh(ppy)$_2$**L2**]PF6 **(Rh2)** (ppy = 2-phenylpyridine, **L1** = 4-(1H-imidazo[4,5-f][1,10]phenanthrolin-2-yl)-*N*,*N*-diphenylaniline, **L2** = N-(4-(1H-imidazo[4,5-f][1,10]phenanthrolin-2-yl) phenyl)-4-methyl-N-(p-tolyl)aniline) have been synthesized and characterized. Both complexes display stronger anticancer activity against a various of cancer cells than cisplatin and they can effectively localize to mitochondria. Further mechanism studies show that **Rh1** induce caspase-dependent apoptosis through mitochondrial damage, down-regulate the expression of B-cell lymphoma-2 (Bcl-2)/Bcl2-associated x (Bax) and reactive oxygen species (ROS) elevation. Our work provides a strategy for the construction of highly effective anticancer agents targeting mitochondrial metabolism through rational modification of rhodium complexes.

1. Introduction

Since the discovery of the anticancer properties and its successful introduction in the clinic in 1969, cisplatin and its analogues are frequently used for the treatment for many cancers, including ovarian, bladder, cervical, testicular, lung cancers as well as lymphomas, myelomas and melanoma [1,2]. However, cisplatin has been severely limited by the dose-limiting side-effects, including nephrotoxicity, neurotoxicity and nausea [3]. To address this, the development and utilization of non-platinum metal complexes with high antitumor activities have been promoted [4,5]. Among them, rhodium(III) complexes have recently attracted much interest due to their chemical and biological properties as well as various pharmacology properties [6–10]. Rhodium(III) complexes have stable [11], diverse ligand structures [12,13], and can bind to biomolecules in cells [14–16], disrupt cell metabolism and produce antitumor effects. Ma's group has reported a series of cyclometalated rhodium complexes, which can inhibit the dimerization of the signal transducer and activator of transcription 3 (STAT3) pathway, thereby inhibiting the proliferation of cancer cells [17]. Chen et al. have reported some rhodium complexes containing isoquinolines, which target mitochondria and increase the level of mitochondria's reactive oxygen species (ROS) to produce significant antitumor effects [18]. The rhodium(III) complex with benzimidazole designed by Fatemeh et al. shows a strong binding effect with DNA and protein, resulting in significant antitumor activity [14]. However, due to the low fluorescence quantum yields of rhodium(III) complexes, they cannot be imaged in cells by optical imaging. To address this, imidazole-based triphenylamino (TPA) derivatives have aroused the researcher's attention because of their good fluorescent properties [19–21], and their intense interaction with cell biological molecules to produce antitumor effects [22,23]. Complexes containing imidazole triphenylamino ligands may enhance the fluorescence performance of rhodium(III) complexes significantly.

Keeping this in mind, in this work, we synthesized and characterized two rhodium(III) complexes, **Rh1** and **Rh2**, with different TPA substituted ligands (Fig. 1). The in vitro antiproliferative activities of these two complexes were investigated against several cancer cell lines as well as a human normal cell line. The anticancer properties of the mitochondria-accumulated complex **Rh1** which included mitochondrial damage, cellular intracellular adenosine triphosphate (ATP) depletion, ROS elevation and induction of apoptosis, were explored using a variety of methods. Additionally, the possible anticancer mechanisms of **Rh1** were elucidated by analysis of the expression of proteins related to the mitochondrial death pathway.

* Corresponding authors.
E-mail addresses: tancaip@mail.sysu.edu.cn (C.-P. Tan), zhaoping666@163.com (P. Zhao).

https://doi.org/10.1016/j.jinorgbio.2021.111400
Received 22 November 2020; Received in revised form 9 February 2021; Accepted 13 February 2021
Available online 25 February 2021

2. Experimental section

2.1. Materials

All reagents were used as received from commercial sources unless otherwise stated. 1,10-phenanthroline-5,6-dione, 4-(diphenylamino) benzaldehyde, 4-(di-p-tolylamino) -benzaldehyde, cisplatin, 3-(4,5-dimethyl-2-thiazolyl)-2,5-diphenyl-2-H-tetrazolium bromide (MTT),

Bcl2-associated x (Bax), B-cell lymphoma-2 (Bcl-2) and Caspase-9, cytochrome C and β-actin antibay, 5,5′,6,6′-tetrachloro-1,1′,3,3′-tetraethyl benzimidazolylcarbocyanine iodide (JC-1), 2,7-dichlorodihydro fluorescein diacetate (H_2DCFDA) and Annexin V-fluorescein Isothiocyanate (Annexin V-FITC) /Propidium Iodide (PI) apoptosis detection kit, MitoTracker Deep Red (MTDR) were obtained from Beyotime (Shanghai, China). HeLa (human cervical cancer), A549 (human lung cancer), MDA-MB-231 (Human breast cancer) cells and MCF-10A (human normal mammary epithelial cell lines) were obtained from Experimental Animal Center of Sun Yat-Sen University (Guangzhou, China). Cells were incubated with Dulbecco's modifed Eagle medium (DMEM) (Gibco BRL) or Roswell Park Memorial Institute (RPMI) 1640 (Gibco BRL) medium which containing 10% fetal bovine serum (FBS, Gibco BRL), 100 IU/mL streptomycin, 100 IU/mL penicillin at 37 °C in 5% CO_2 and 95% air.

2.2. General instruments

Electrospray ionization mass spectra (ESI-MS) were detecting by an LCQ system (Finnigan MAT, USA). ^{1}H and ^{13}C NMR spectra were detected by a Varian Mercury Plus 400 Nuclear Magnetic Resonance Spectrometer and 500 Nuclear Magnetic Resonance Spectrometer, respectively. Microanalysis (C, H, and N) was carried out using an Elementar Vario EL elemental analyzer. The electronic absorption spectra were detected by a Perkin-Elmer Lambda 850 UV/Vis spectrometer. The emission spectra were detected by a Perkin-Elmer LS 55 luminescence spectrometer. Inductively coupled plasma mass spectrometry (ICP-MS) were detected by an iCAP RQ (Thermo Fisher) spectrometer. Confocal microscopy images were detected by LSM 710 NLO (Zeiss) microscope. Flow Cytometry was carried out on a BD FACS Canto II flow cytometer.

2.3. Synthesis of ligands and its corresponding rhodium(III) complexes

The chloro-bridged dinuclear rhodium(III) precursor $[Rh(ppy)_2]_2Cl_2$ was synthesized according to the literature [13]. The ligand of 4-(1H-imidazo[4,5-f][1,10]phenanthrolin-2-yl)-*N*,*N*-diphenylaniline (**L1**) was synthesized according to the literature [19]. The ligand N-(4-(1H-imidazo[4,5-f][1,10]phenanthrolin-2-yl)phenyl)-4-methyl-N-(p-tolyl)aniline (**L2**) was synthesized according to the literature [24].

2.3.1. Synthesis of $[Rh(ppy)_2L1]PF_6$ (Rh1)

The ligand **L1** (0.093 g, 0.2 mmol) and $[Rh(ppy)_2Cl]_2$ (0.091 g, 0.1 mmol) were placed in a 50 mL round bottomed flask with 30 mL of dichloromethane (CH_2Cl_2) and methanol (2: 1, *v*/v). The mixture was heated at 50 °C for 4 h under nitrogen. Then the mixture was cooled to room temperature, and the solvent was evaporated under reduced pressure. After that, the mixture was mixed with saturated aqueous NH_4PF_6, followed by stirring for 2 h. The crude product was purified by column chromatography on silica using CH_2Cl_2-methanol (100:1, *v*/v) as the eluent , giving the product as a yellow powder (0.130 g, 62%). ESI-MS: 875.05 $[M - PF_6]^+$. ^{1}H NMR (500 MHz, DMSO) δ 14.12 (s, 1H), 9.19 (d, J = 7.2 Hz, 2H), 8.29 (d, J = 8.2 Hz, 2H), 8.17 (d, J = 7.3 Hz, 4H), 8.03 (t, J = 12.8 Hz, 4H), 7.96 (t, J = 7.8 Hz, 2H), 7.48 (d, J = 5.1 Hz, 2H), 7.39 (t, J = 7.8 Hz, 4H), 7.19–7.12 (m, 10H), 7.04 (dd, J = 16.0, 8.0 Hz, 4H), 6.31 (d, J = 7.6 Hz, 2H). ^{13}C NMR (126 MHz, DMSO) δ 168.15, 167.89, 164.68, 153.26, 149.98, 149.55, 148.06, 144.45, 144.34, 143.05, 139.27, 133.95, 132.77, 132.69, 130.79, 130.46, 128.19, 127.00, 125.80, 125.34, 124.34, 123.64, 121.86, 120.67, 20.55. Elemental analysis: calcd (%) for $C_{53}H_{37}F_6N_7PRh\bullet H_2O$: C, 61.34; H, 3.79; N, 9.45; found: C, 61.43; H, 3.73; N, 9.34.

2.3.2. Synthesis of $[Rh(ppy)_2L2]PF_6$ (Rh2)

This complex was synthesized according to a similar procedure with **Rh1**, giving the product as a yellow powder (0.140 g, 67%). ESI-MS: 903.00 $[M - PF_6]^+$. ^{1}H NMR (500 MHz, DMSO) δ 14.08 (s, 1H), 9.26–9.09 (m, 2H), 8.29 (d, J = 8.1 Hz, 2H), 8.18 (d, J = 12.9 Hz, 2H), 8.14–8.09 (m, 2H), 8.03 (t, J = 14.9 Hz, 4H), 7.96 (t, J = 7.5 Hz, 2H), 7.48 (s, 2H), 7.19 (d, J = 8.1 Hz, 4H), 7.14 (t, J = 7.5 Hz, 2H), 7.04 (q, J = 8.8 Hz, 10H), 6.32 (d, J = 7.6 Hz, 2H), 2.31 (s, 6H). ^{13}C NMR (126 MHz, DMSO) δ 168.15, 167.89, 164.68, 153.26, 149.98, 149.55, 148.06, 144.45, 144.34, 143.05, 139.27, 133.95, 132.77, 132.69, 130.79, 130.46, 128.19, 127.00, 125.80, 125.34, 124.34, 123.64, 121.86, 120.67, 20.55. Elemental analysis: calcd (%) for $C_{55}H_{41}F_6N_7PRh\bullet H_2O$: C, 61.98; H, 4.07; N, 9.20; found: C, 61.67; H, 4.10; N, 9.20.

2.4. Cell cytotoxicity

The cells were cultured in 96-well tissue culture plates at a density of 10, 000 cells per well for 12 h. Then, the cells were incubated with varies concentrations of the compounds for 68 h. 20 μL of MTT (5 mg/mL) was then added to each well, and the plates were incubated for another 4 h. The media was carefully removed and 150 μL dimethyl sulfoxide (DMSO) was added per well and incubated for 10 min with shaking. The absorbance was measured using a microplate reader. For the cytotoxicity assay in the presence of the inhibitors, HeLa cells were pre-incubated with 10 mM *N*-acetyl-L-cysteine (NAC) or 50 μM *Z*-Val-Ala-Asp(OMe)-FMK (z-VAD-FMK) for 1 h, and then treated with **Rh1** at the indicated concentrations for 36 h. The cell viability was tested by measurement of the absorbance at 570 nm (Infinite F200, Tecan, Switzerland).

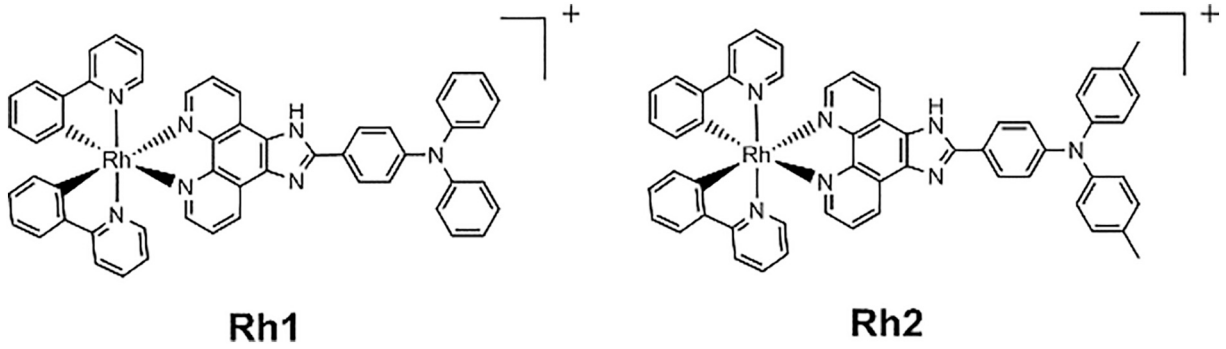

Fig. 1. Chemical structures of Rh(III) complexes.

2.5. Lipophilicity measurement

The lipophilicities of **Rh1** and **Rh2** were tested according to the previously reported method [25]. Octanol-saturated water (W) and water-saturated octanol (O) were acquired by mixing octanol and water. Aliquots of stock solutions of the rhodium complexes in W were added to equal volumes of O and were shaken at 1000 rpm for 72 h. Then the sample was centrifuged at 8000 rpm for 3 min. The aqueous and octanol layers were carefully separated into test tubes and measured by UV–Vis spectroscopy. Partition coefficients of ruthenium complexes were calculated using the eq. (1):

$$logP = log([RhO]/[RhW]) \quad (1)$$

2.6. Cell colocalization assay

HeLa cells were cultured in confocal microscopy dishes and incubated for 12 h. Rhodium complexes were added to the dishes and incubated with the cells at 37 °C for 2 h. The cells were then incubated with MitoTracker Deep Red (MTDR) (100 nM) for 0.5 h. After that, the cells were washed by phosphate buffer saline (PBS). The cells were imaged with a Zeiss LSM 710 NLO confocal microscope (63 × oil). **Rh1** and **Rh2**: $\lambda_{ex} = 405$ nm; $\lambda_{em} = 600 \pm 20$ nm. MTDR: $\lambda_{ex} = 633$ nm, $\lambda_{em} = 650 \pm 20$ nm.

2.7. ICP-MS analysis

HeLa cells were cultured in 10 cm culture plates for 12 h. Then, they were incubated with the rhodium complexes (2 μM) at 37 °C for 6 h. The cytoplasmic, mitochondrial and nuclear were obtained using the commercial kit (Beyotime, China). The rhodium concentration in the subcellular compartments was determined using ICP-MS (Thermo Elemental Co., Ltd). The data are reported as the mean ± standard deviation ($n = 3$).

2.8. Mitochondrial membrane potential assay

HeLa cells were cultured in 6-wells plates incubated for 12 h. **Rh1** with different concentrations were added to the wells and incubated with the cells at 37 °C for 12 h. The cells were then washed by fresh medium three times. Then, the working buffer for JC-1 staining was added and the cells followed by incubating for 20 min. The fluorescence was recorded by Flow cytometer. $\lambda_{ex} = 488$ nm; $\lambda_{em} = 580 \pm 20$ nm (Red); $\lambda_{em} = 510 \pm 20$ nm (Green).

2.9. Intracellular ROS detection

HeLa cells were cultured in 6-wells plates incubated for 24 h. Then **Rh1** at the indicated concentrations were added and incubated for 12 h. The cells were harvested and incubated with 10 μM H_2DCFDA for 30 min at 37 °C in the dark. The cells were collected by centrifugation and washed twice with serum-free DMEM to remove the excess staining dye. The 2′,7′-dichlorofluorescein (DCF) fluorescence intensity of cell was detected by flow cytometry. $\lambda_{ex} = 488$ nm; $\lambda_{em} = 530 \pm 30$ nm. The mean fluorescence intensity (MFI) was analyzed using FlowJo 7.6 software.

2.10. Colocalization assay of DCF and MTDR

HeLa cells were cultured in confocal microscopy dishes incubated for 12 h and then treated with **Rh1** (2 μM) for another 6 h. The colocalization of the fluorescence of DCF and MTDR was obtained as previously described [26]. MTDR: $\lambda_{ex} = 633$ nm; $\lambda_{em} = 650 \pm 20$ nm. DCF: $\lambda_{ex} = 488$ nm; $\lambda_{em} = 510 \pm 20$ nm.

2.11. ATP depletion assay

ATP quantification was detected using CellTiter-Glo® Luminescent Cell Viability Assay kit (G7570, Promega, USA) according to the manufacturer's instructions. HeLa cells were plated at a density of 1.4×10^5 cells/mL in 96 well plates and incubated for 24 h and then incubated with **Rh1** at the indicated concentrations for another 12 h. The culture medium was extracted for 100 mL, and then 100 mL of cellTiter-Glo reagent was added to each well, incubated for another 10 min at room temperature. The luminescence was measured employing a microplate reader (Infinite M200 Pro, Tecan, Switzerland).

2.12. Hoechst 33342 staining

HeLa cells were cultured in confocal microscopy dishes for 12 h, and then treated with **Rh1** at the indicated concentrations for 24 h. Cells were washed twice with cold PBS and fixed with 4% paraformaldehyde at room temperature for 2 h. After the cells were labeled with 2′-(4-ethoxyphenyl)-5-(4-methyl-1-piperazinyl)-1H,3′H-2,5′-bibenzimidazole (Hoechst 33342, 5 μg/mL in water) for 30 min, they were analyzed immediately by confocal microscopy. $\lambda_{ex} = 405$ nm, $\lambda_{em} = 460 \pm 20$ nm.

2.13. Annexin V/PI staining

HeLa cells were cultured in 6-wells plates for 12 h and treated with **Rh1** at the indicated concentrations for 24 h. Cells were collected by centrifugation and washed twice with cold PBS. The resuspended cells were incubated with Annexin V-FITC and PI for 30 min in the dark at 37 °C. Data were collected by a flow cytometer. Annexin V ($\lambda_{ex} = 488$ nm, $\lambda_{em} = 510 \pm 20$ nm), PI ($\lambda_{ex} = 488$ nm, $\lambda_{em} = 610 \pm 20$ nm) (FACSCaliburTM, Becton Dickinson, Franklin Lakes, NJ, USA) and analyzed with FlowJo 7.6 software (Tree Star, OR, USA).

2.14. Western blot analysis

HeLa cells were plated at 10 cm culture plates and treated with **Rh1** at indicated concentration for 24 h. The cells were collected and washed three times using PBS, then incubated with radioimmuno precipitation assay buffer (RIPA) at 4 °C for 30 min, and the protein concentrations were ascertained by UV. Equal amounts of cellular total proteins were resolved by SDS-polyacrylamide gel electrophoresis and transferred to nitrocellulose membranes. The membranes were blocked with 5% blocking buffer at room temperature for 2 h, and then incubated overnight at 4 °C with β-actin, Bcl-2, Bax, Caspase-9 and cytochrome C primary antibodies, followed by incubation with HRP-conjugated secondary antibody for 2 h at room temperature. An enhanced chemiluminescence kit was using for detection using Image Lab software (Bio-Rad Gel Doc XR+).

2.15. Statistical analysis

All biological experiments were performed at least twice with triplicates in each experiment. Representative results are presented as the means ± standard deviations.

3. Results and discussion

3.1. Synthesis and characterization

Rh1 and **Rh2** were successfully synthesized using a facile method with high yields. The synthetic routes of the ligands and complexes are elucidated in Scheme. S1. The complexes were characterized by ESI-MS, ^{1}H NMR, ^{13}C NMR and elemental analyses (Fig. S1-S6). The UV–Vis absorption spectra of **Rh1** and **Rh2** were detected in CH_2Cl_2, acetonitrile (CH_3CN) and PBS, respectively (Fig. 2A). The results clearly reveal that intense spin-allowed intragand transition ($\pi \rightarrow \pi^*$) absorption bands at

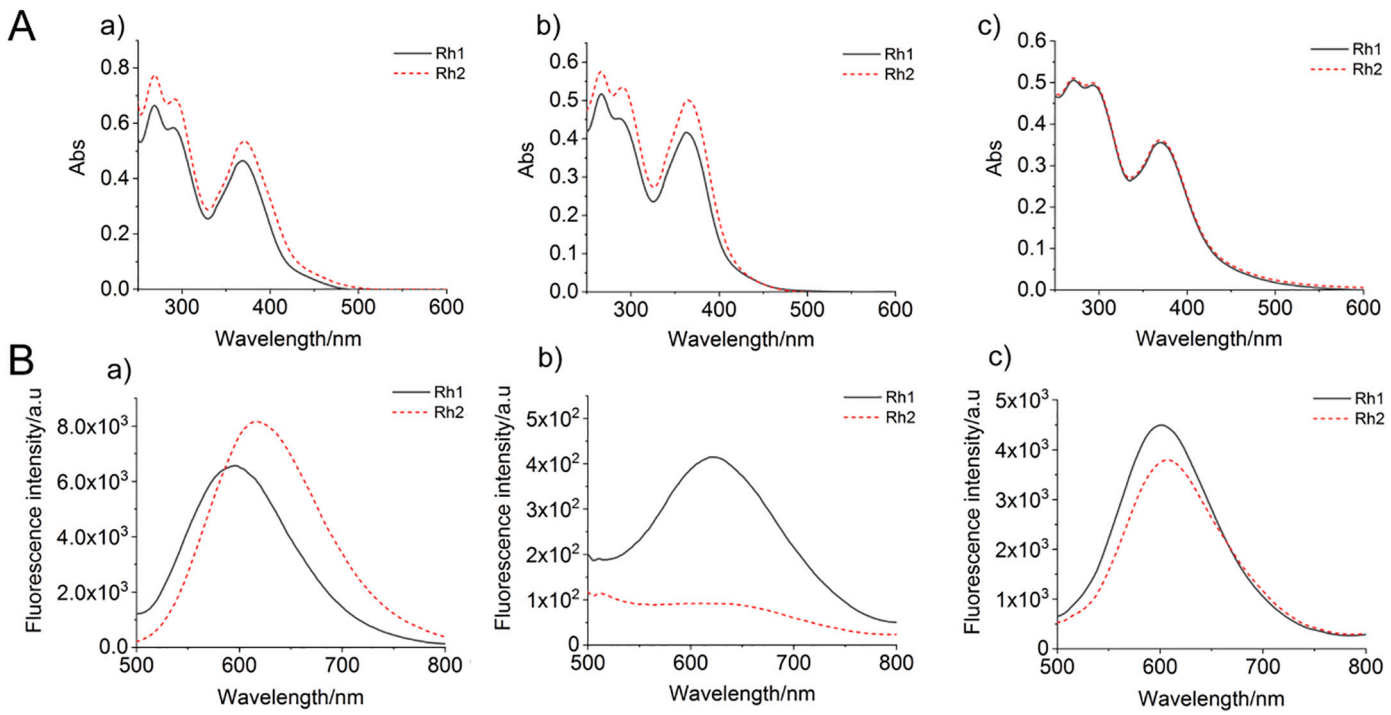

Fig. 2. A) UV–Vis spectra of **Rh1** and **Rh2** in CH_2Cl_2 (a), CH_3CN (b) and PBS (c). B) Emission spectra of **Rh1** and **Rh2** (λ_{exc} = 405 nm) in CH_2Cl_2 (a), CH_3CN (b), PBS (c) at 25 °C.

approximately 250–340 nm in the UV region and less intense spin-allowed metal-to-ligand charge-transfer (MLCT) absorption bands at approximately 350–530 nm [27,28], respectively. These are the characteristic bands of rhodium complexes, suggesting the successful coordination of the metal. In addition, no obvious change can be observed in the time-dependent absorption spectra of **Rh1-Rh2** (Fig. S7), indicating the high stability of these two complexes.

The emission spectra (Fig. 2B) and the phosphorescence lifetimes of **Rh1** and **Rh2** in the indicated solutions were detected (Table S1).Upon excitation at 405 nm, **Rh1** and **Rh2** display yellow-red emission with an emission maximum around 600 nm. The emission intensities of **Rh1** and **Rh2** show a dependence on the polarity of the solvents, with no spectral shift observed.

Meanwhile, lipophilicity is commonly referred to as the partition coefficient of the compound in n-octanol/water ($P_{o/w}$). The lipophilicity of **Rh1** and **Rh2** was measured by the classical shake-flask method. The log$P_{o/w}$ values of **Rh1** and **Rh2** are 1.74 and 2.27, respectively. As expected, the lipophilicity of the complexes increases with adding a methyl group on the benzene ring. This result is consistent with the conclusion drawn by the previous reports [29].

3.2. Cytotoxicity studies

The cytotoxicity of **Rh1** and **Rh2** were tested by MTT assay against HeLa, A549 MDA-MB-231 and MCF-10A cells. The IC_{50} (50% inhibition of cell growth) values of **Rh1** and **Rh2** after an incubation with the indicated cells for 72 h are listed in Table 1 and the survival curves are given in Fig. S8. **Rh1** and **Rh2** show higher cytotoxicities than cisplatin against all the cell lines tested. Notably, **Rh1** and **Rh2** show a lower cytotoxicity to human normal MCF-10A cells than to those cancer cells. The cytotoxicity potency of Rh(III) complexes are opposite to their lipophilicity, which may result from the fact that the benzene substituents in **Rh1** have stronger molecular interaction with biomolecular targets than the methyl substituents in **Rh2** [30,31]. Since **Rh1** shows a higher anticancer potency than **Rh2,** we chose **Rh1** for further investigation regarding the underlying mechanisms of anticancer activities.

Table 1
Cytotoxicity (IC_{50}) of **Rh1** and **Rh2** towards cells in vitro.[a]

Complex	IC_{50} (μM)			
	HeLa	A549	MDA-MB-231	MCF-10A
Rh1	1.13 ± 0.03	1.77 ± 0.04	0.74 ± 0.02	4.57 ± 0.10
Rh2	2.10 ± 0.20	2.97 ± 0.20	1.58 ± 0.04	8.78 ± 0.31
Cisplatin	8.91 ± 0.20	7.53 ± 0.43	7.08 ± 0.16	14.13 ± 0.32

[a] IC_{50} values are drug concentrations necessary for 50% inhibition of cell viability. Data are presented as means ± standard deviations obtained in at least three independent experiments. Cells are treated with the complexes for 72 h.

3.3. Cellular uptake and localization

Since both **Rh1** and **Rh2** emit phosphorescence at 600 nm (Table S1), their cellular distribution was investigated by confocal microscopic observation. Both the two complexes can be visualized in the HeLa cells after 2 h incubation (Fig. 3). Colocalization experiments with the mitochondrion-specific fluorescent probe MTDR show that **Rh1** and **Rh2** can specifically localize to mitochondria (Fig. 3). The Pearson's colocalization coefficients obtained for **Rh1** and **Rh2** with MTDR are 0.90 and 0.88, respectively, indicating that both **Rh1** and **Rh2** can effectively target mitochondria.

To further verify the distribution of **Rh1** and **Rh2** in different cellular compartments, the mitochondrial, cytosolic and nuclear fractions were isolated from HeLa cells treated with complexes **Rh1** and **Rh2** (Fig. 4). As measured by ICP-MS, the contents of rhodium (III) in the in the mitochondria is much higher than that obtained in the cytosol and nuclei. These results collectively indicate that complexes **Rh1** and **Rh2** can specifically target mitochondria in HeLa cells. The results indicate that both **Rh1** and **Rh2** have much higher accumulated levels in mitochondria compare with cytoplasm and nucleus.

3.4. Mitochondrial damage

The cell uptake results indicate that the studied **Rh1-Rh2** complexes

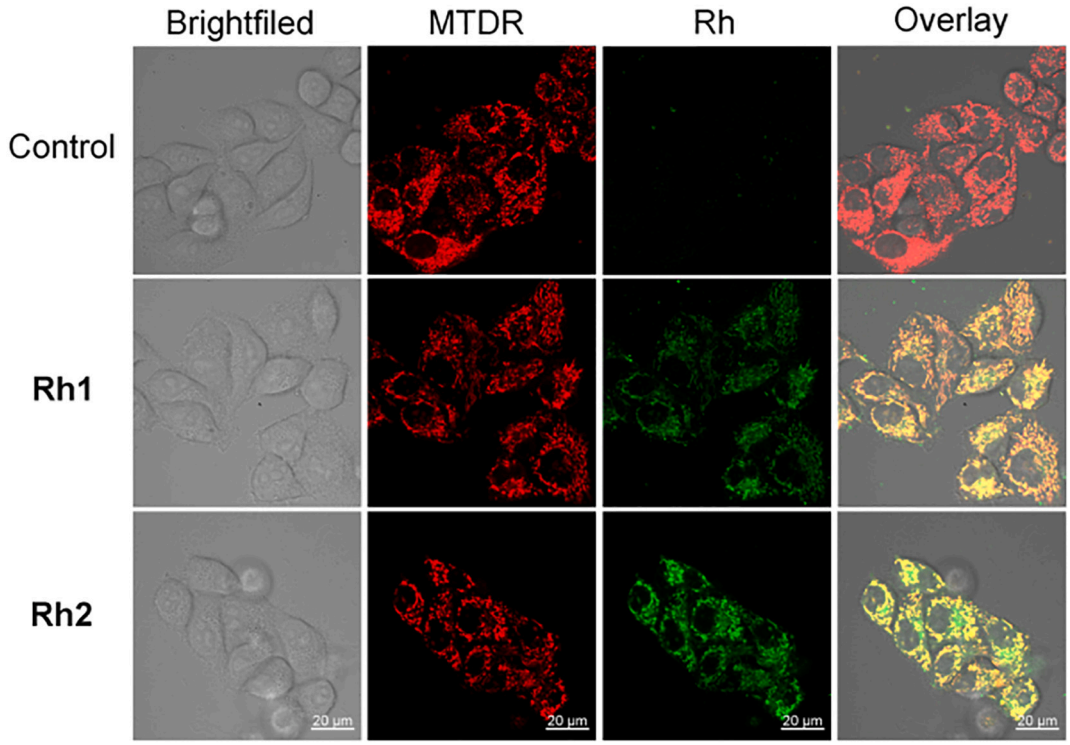

Fig. 3. Determination of intercellular colocalization of **Rh1** and **Rh2** with MTDR by confocal microscopy. HeLa cells were incubated with **Rh1** and **Rh2** (2 μM, 2 h), and then stained with MTDR (100 nM, 0.5 h) at 37 °C. MTDR (λ_{ex} = 633 nm, λ_{em} = 650 ± 20 nm). **Rh1**-**Rh2** (λ_{ex} = 405 nm, λ_{em} = 600 ± 20 nm).

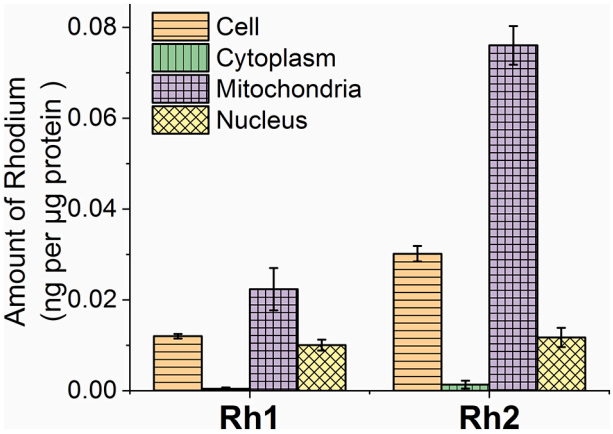

Fig. 4. Distribution of complexes **Rh1-Rh2** in cellular compartments of HeLa cells measured by ICP-MS. **Rh1** (2 μM) and **Rh2** (2 μM) were with incubated HeLa cells for 6 h at 37 °C, and then were isolated from the cytoplasmic, mitochondrial and nuclear using the corresponding commercial kits.

are mainly localized in mitochondria. Mitochondrion is the energy production center of the cell, and it is also an essential component of apoptotic signaling pathway in cell [32,33]. The pro-death factors are released from mitochondria, and initiate cell death signal when the membrane integrity of mitochondria is damaged [34].

As complexes **Rh1-Rh2** could be localized to mitochondria, their impact on mitochondrial integrity was monitored by detecting the changes in mitochondrial membrane potential (MMP). The red/green fluorescence of JC-1, a mitochondria-selective aggregate dye, was detected by flow cytometry (Fig. 5A). At low membrane potentials, JC-1 exists in the form of the "J-monomer" with green fluorescence. At high membrane potentials, JC-1 forms "J-aggregates" and displays red fluorescence. The control cells show red fluorescence, which indicates that the mitochondrial membranes retain a high voltage. HeLa cells treated with complex **Rh1** show a concentration-dependent red to green color shift in JC-1 fluorescence, and the percentage of cells with depolarized mitochondrial membranes increases from 8.3% to 54.4%. The results indicate that MMP of **Rh1**-treated cells are significantly decreased. To further investigate the effects of **Rh1** on mitochondrial metabolic status, we detected the intracellular ATP level of the cancer cells treated with Rh(III) complex. The results show that **Rh1** cause a significant dose-dependent decrease in ATP production as compared with the control cells (Fig. 5B). The ATP levels decrease to 78.7%, 64.7% and 54.5% for 1 μM, 2 μM and 4 μM, respectively, confirming the cellular mitochondrial damage by the designed Rh(III) complexes.

3.5. Real-time tracking of mitochondrial morphology

In living cells, mitochondrial integrity plays a vital role in maintaining cell function [35,36]. Mitochondrial morphology and functions are closely linked, and mitochondrial morphological changes are associated with many vital cellular functions [33]. Mitochondria changes in number and morphology of mitochondria are often observed when they are damaged. Thus, the therapeutic effect can be monitored by real-time tracking of the mitochondrial morphological changes in cells.

Real-time tracking of the mitochondrial morphology change was performed by monitoring the emission of MTDR in HeLa cells treated with **Rh1** using confocal microscopy (Fig. 6). The MTDR phosphorescence presents a filamentous distribution at first, which is the normal mitochondrial morphology of cells. With the prolonged incubation with **Rh1**, mitochondria gradually become swelling, fragmentation and perinuclear clustering in cells. This result indicates that the designed **Rh1** can damage the mitochondria of the cells, which may contribute to the anticancer activity of the rhodium complexes.

3.6. Intracellular ROS detection

It is well known that mitochondria is not only a source of energy, but

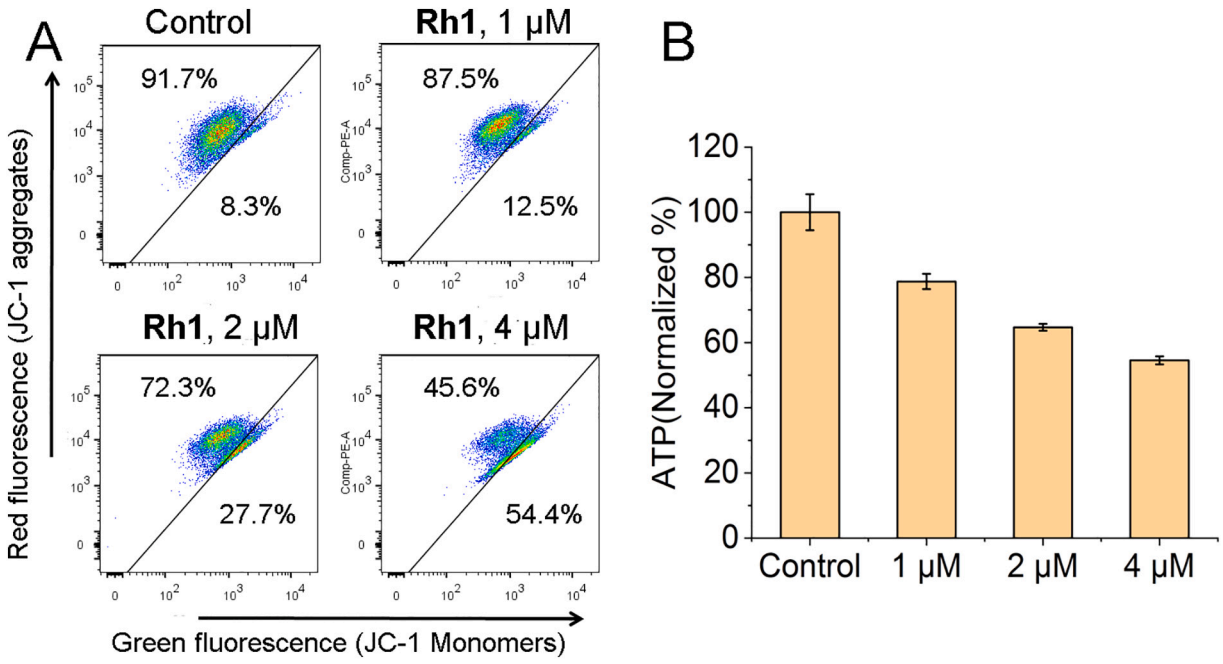

Fig. 5. A) Effects of **Rh1** on MMP analyzed by JC-1 staining and flow cytometry. HeLa cells were treated with **Rh1** at the indicated concentrations for 12 h at 37 °C. JC-1 monomers (Green): $\lambda_{ex} = 488$ nm, $\lambda_{em} = 510 \pm 20$; JC-1 aggregates (Red): $\lambda_{ex} = 488$ nm, $\lambda_{em} = 580 \pm 20$ nm. B) Intracellular ATP levels in HeLa cells. HeLa cells were treated with **Rh1** at the indicated concentrations for 12 h at 37 °C. (For interpretation of the references to color in this figure legend, the reader is referred to the web version of this article.)

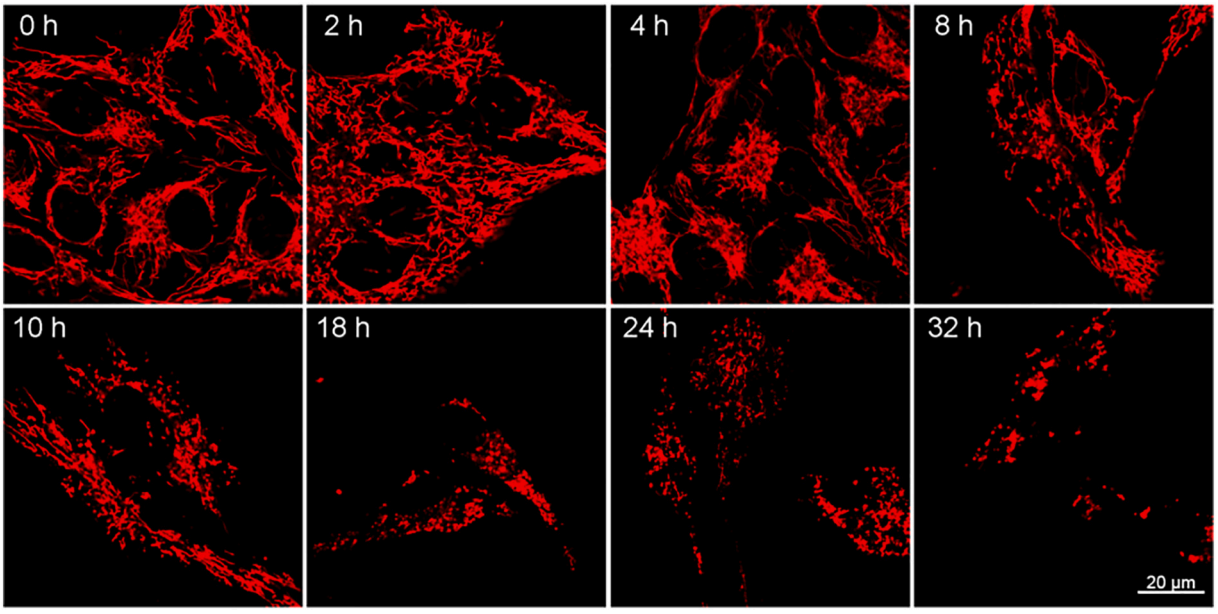

Fig. 6. Real-time tracking of mitochondria in HeLa cells stained with **Rh1** (2 μM) over a period of 32 h. MTDR were excited at 633 nm and the phosphorescence was collected at 650 ± 20 nm.

also a major source of ROS [37]. Elevated intracellular ROS levels and mitochondrial damage are closely related to events in cell death [38,39]. The effects of **Rh1** on intracellular ROS levels of HeLa cells were detected by DCF assay using flow cytometry (Fig. 7A). After a 12 h treatment with **Rh1**, the MFI of DCF in HeLa cells exhibits a dramatic concentration dependent ROS elevation, increasing to approximately 9.77- fold at 4 μM of **Rh1**. Moreover, the overlap between the fluorescence of DCF and MTDR shows that ROS are mainly generated in mitochondria (Fig. 7B). In addition, as an efficient quencher of ROS, NAC is frequently employed in the mechanism research of ROS-related anticancer activity. As shown in Fig. 7C, the viability of HeLa cells pretreated with NAC was significantly reduced as compared with cells treated with **Rh1** alone. These results indicate that **Rh1** induces ROS-dependent cell death.

3.7. Induction of apoptosis

Mitochondria play a vital role in the adjusting of intrinsic pathway for the apoptosis of cells [35,40], and regulate the cell apoptosis through the release of a different mitochondrial proteins where is

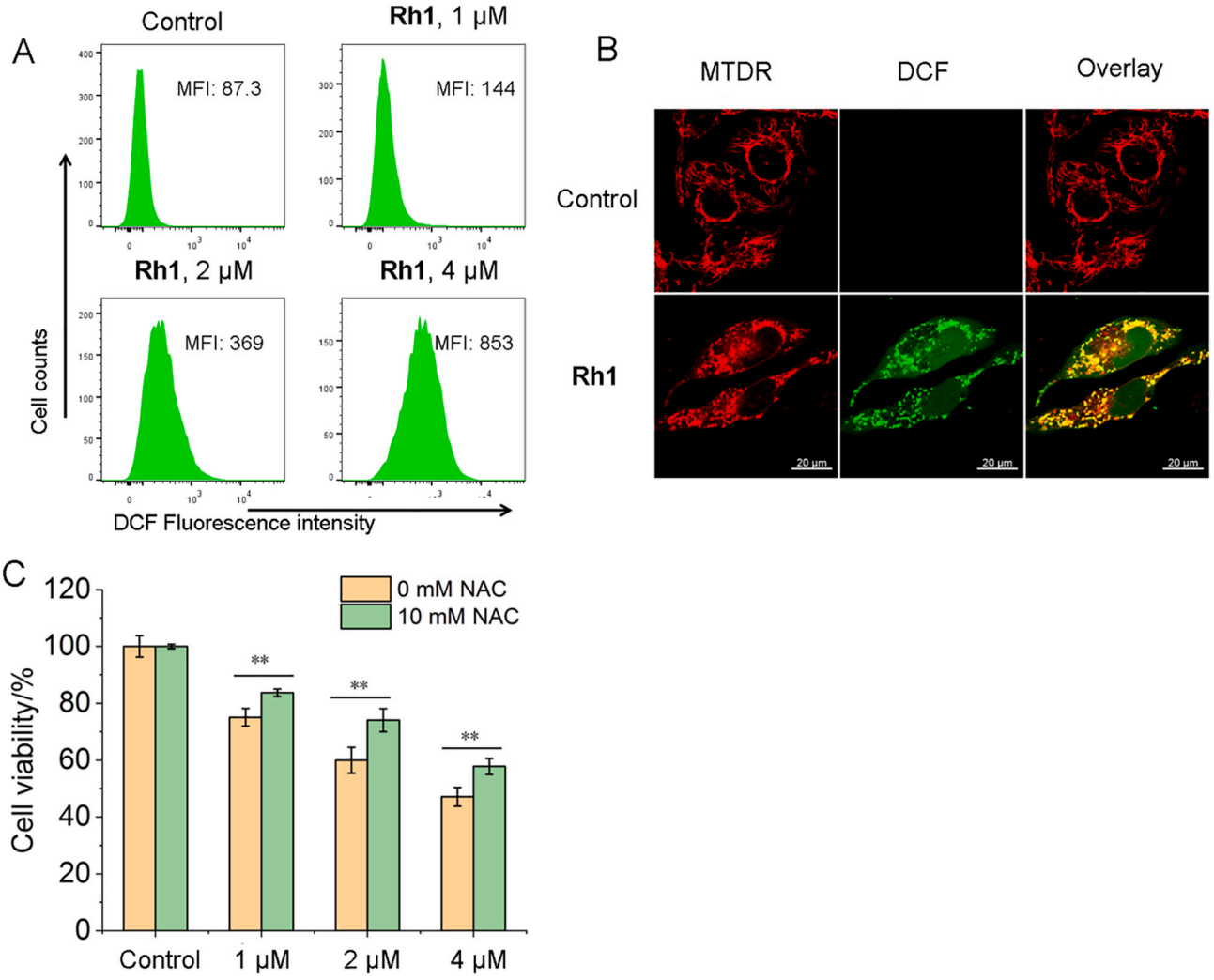

Fig. 7. A) Analysis of ROS levels by flow cytometry after HeLa cells were treated with **Rh1** at the indicated concentrations for 12 h and stained with H_2DCFDA. B) Generation of mitochondrial ROS caused by **Rh1** treatment. HeLa cells were treated with **Rh1** at 2 μM for 6 h. Then the cells were co-stained with H_2DCFDA and MTDR for confocal microscopic observation. DCF: λ_{ex} = 488 nm; λ_{em} = 530 ± 20 nm; MTDR: λ_{ex} = 633 nm; λ_{em} = 650 ± 20 nm. C) The impact of NAC on the cytotoxicity of **Rh1**. HeLa cells were treated with **Rh1** for 36 h at the indicated concentrations in the absence or presence of NAC. Cell viability was measured by MTT assay. Data are represented as means ± SD of three independent experiments. $^{**}p < 0.02$.

intermembrane space, which leads to activation of caspases [41,42]. Apoptosis is usually characterized by a series of prominent morphological features, such as phosphatidylserine externalization, activation of caspase family proteases, cytoplasmic shrinkage, plasma membrane blebbing, chromatin condensation or nuclear fragmentation [43,44]. Change in nuclear morphology treated with **Rh1** was firstly investigated by Hoechst 33342 staining by confocal microscopy.

As shown in Fig. 8A, drug-treated control cells show normal overall morphology and a homogeneous nuclear staining pattern. After treated with **Rh1** at indicated concentration for 24 h, the cells show distinct morphologic signals of apoptosis in a concentration-dependent manner. Most of the cells display typical morphological changes that are characteristic of apoptosis, which including cell shrinkage, membrane bubbling, staining bright, condensed chromatin and fragmented nuclei.

During apoptosis, phosphatidylserine externalization is considered to be a hall-mark of early apoptosis. Early apoptotic cells are annexin V-positive but PI-negative because phosphatidylserine is externalized while the plasmic membrane is integrated. Both late apoptotic and necrotic cells can be double stained by annexin V and PI. Flow cytometric determined shows that treatment of HeLa cells with **Rh1** leads to a dose-dependent increase in the percentage of apoptotic cells (Fig. 8B). After treated with **Rh1** for 24 h, the percentages of HeLa cells in apoptotic phase (annexin V-positive) increase from 3.42% (control) to 10.98% (1 μM), 16.98% (2 μM), and 43.8% (4 μM) of the complex, respectively, demonstrating that **Rh1** can induce a dose-dependent apoptosis for cancer cells.

Mitochondria control the intrinsic pathway of apoptosis by regulating the translocation of pro-apoptotic proteins, e.g., cytochrome C, from mitochondrial intermembrane space to cytosol [45,46]. The release of cytochrome C proteins from mitochondria can activate death-driving proteolytic proteins known as caspases. The Bcl-2 family of proteins [35,41,47], consisting of anti-apoptotic and proapoptotic members, regulate MMP and mitochondrial perme-ability during apoptosis [47]. Therefore, we investigated the effect of **Rh1**-treatment on the expression of proteins related to the mitochondrial death pathway using Western blotting. Cytochrome C, Caspase-9, Bcl-2, and Bax, are known to play vital roles in the mitochondrial cell death pathway. As shown in Fig. 8C, the results show that **Rh1** can elevate the expression level of Bax and Caspase-9, and promote the release of cytochrome C proteins from mitochondria to cytosol. Moreover, **Rh1** can reduce the expression level of Bcl-2. The down-regulated Bcl-2/Bax ratio induced by **Rh1** promotes the cellular apoptosis.

To further explore the mechanism of cell apoptosis, z-VAD-FMK, a well-accepted caspase inhibitor, is employed to pretreat the HeLa cells.

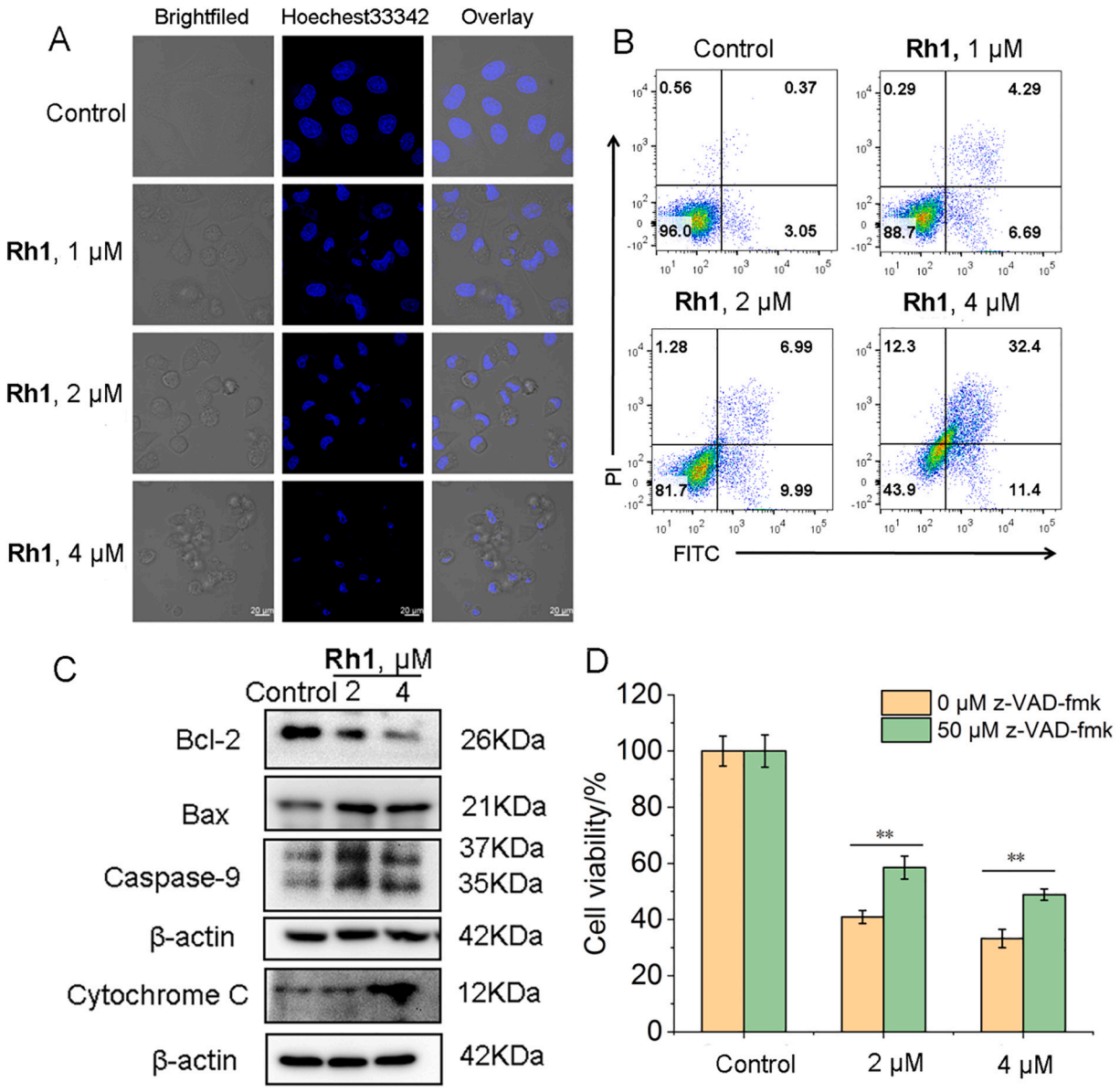

Fig. 8. A) Detection of apoptosis in HeLa cells stained with Hoechst 333342 after treatment with **Rh1** for 24 h at the indicated concentrations by confocal microscopy. Hoechst 33342: λex = 405 nm; λem = 450 ± 20 nm. B) Detection of apoptosis in HeLa cells stained with annexin V and PI after treatment with **Rh1** for 24 h at the indicated concentrations by Flow cytometric. Annexin V (λex = 488 nm, λem = 510 ± 20 nm), PI (λex = 488 nm, λem = 610 ± 20 nm). C) Representative Western blots of the effects of **Rh1** on the protein expression levels of Bcl-2, Bax, Caspase-9 and cytochrome C, β-actin was assessed as a loading control. D) The impact of z-VAD-FMK on the cytotoxicity of **Rh1**. HeLa cells were treated with **Rh1** for 36 h at the indicated concentrations in the absence or presence of z-VAD-FMK. Cell viability was measured by MTT assay. Data are represented as means ± SD of three independent experiments. $^{**}p < 0.02$, compared with the cell viability of **Rh1** treatment alone.

Cells pretreated with z-VAD-FMK (50 μM) show an outstanding increase in cell viability compared with cells treated with **Rh1** alone (Fig. 8D). This result confirmed that the cell death induced by **Rh1** is mainly executed through the caspase-dependent apoptotic pathway, and also show that the damaged mitochondria by rhodium complexes initiates a cascade of events that can result in execution of cell death.

4. Conclusion

Two cyclometalated rhodium(III) complexes containing the TPA moiety were synthesized and characterized, and their in vitro antitumor activities were tested. The TPA moiety endows the Rh(III) complexes good fluorescence properties, and both **Rh1** and **Rh2** show higher antitumor properties than cisplatin against a various of cancer cells. Mechanism investigations indicated that **Rh1** and **Rh2** mainly located in mitochondria, damaged the integrity of mitochondrial membranes and increased the level of ROS in cells. The immunobloting results indicated that cell death induced by **Rh1** is executed through the caspase-dependent apoptotic pathway. Overall, we demonstrate that cyclometalated rhodium(III) complexes are potential leading compounds for further development as anticancer candidates acting through mechanisms different from those of cisplatin.

Authorship contributions

None.

Declaration of Competing Interest

None.

Acknowledgment

This work was supported by the Unique Feature and Innovation Project of Guangdong Province, China (2017KTSCX103), the Social Welfare Projects of Zhongshan (2020B2023) and Guangzhou Key Laboratory of Construction and Application of New Drug Screening Model Systems.

Appendix A. Supplementary data

Supplementary data to this article can be found online at https://doi.org/10.1016/j.jinorgbio.2021.111400.

References

[1] S. Dasari, P.B. Tchounwou, Eur. J. Pharmacol. 740 (2014) 364–378, https://doi.org/10.1016/j.ejphar.2014.07.025.
[2] D.P. Silver, A.L. Richardson, A.C. Eklund, Z.C. Wang, Z. Szallasi, Q. Li, N. Juul, C. O. Leong, D. Calogrias, A. Buraimoh, A. Fatima, R.S. Gelman, P.D. Ryan, N. M. Tung, A. De Nicolo, S. Ganesan, A. Miron, C. Colin, D.C. Sgroi, L.W. Ellisen, E. P. Winer, J.E. Garber, J. Clin. Oncol. 28 (2010) 1145–1153, https://doi.org/10.1200/JCO.2009.22.4725.
[3] X. Yao, K. Panichpisal, N. Kurtzman, K. Nugent, Am.J. Med. Sci. 334 (2007) 115–124, https://doi.org/10.1097/MAJ.0b013e31812dfe1e.
[4] D.L. Ma, D.S. Chan, C.H. Leung, Acc. Chem. Res. 47 (2014) 3614–3631, https://doi.org/10.1021/ar500310z.
[5] U. Jungwirth, C.R. Kowol, B.K. Keppler, C.G. Hartinger, W. Berger, P. Heffeter, Antioxid. Redox. Sign. 15 (2011) 1085–1127, https://doi.org/10.1089/ars.2010.3663.
[6] H.J. Edwards, J.D. Hargrave, S.D. Penrose, C.G. Frost, Chem. Soc. Rev. 39 (2010) 2093–2105, https://doi.org/10.1039/b919762c.
[7] D. Fujita, H. Sugimoto, Y. Morimoto, S. Itoh, Inorg. Chem. 57 (2018) 9738–9747, https://doi.org/10.1021/acs.inorgchem.8b00289.
[8] T.S. Kang, W. Wang, H.J. Zhong, J.X. Liang, C.N. Ko, J.J. Lu, X.P. Chen, D.L. Ma, C. H. Leung, Bba-Gen. Subiects 1861 (2017) 256–263, https://doi.org/10.1016/j.bbagen.2016.11.032.
[9] R.J. Ernst, A.C. Komor, J.K. Barton, Biochemistry. 50 (2011) 10919–10928, https://doi.org/10.1021/bi2015822.
[10] X. Wang, Y. Li, M. Lin, J. Jin, Z. Huang, Biometals. 30 (2017) 903–915, https://doi.org/10.1007/s10534-017-0056-4.
[11] D.L. Ma, M. Wang, Z. Mao, C. Yang, C.T. Ng, C.H. Leung, Dalton Trans. 45 (2016) 2762–2771, https://doi.org/10.1039/c5dt04338g.
[12] X. Lu, Y.M. Wu, J.M. Yang, F.E. Ma, L.P. Li, S. Chen, Y. Zhang, Q.L. Ni, Y.M. Pan, X. Hong, Y. Peng, Eur. J. Med. Chem. 151 (2018) 226–236, https://doi.org/10.1016/j.ejmech.2018.03.074.
[13] H. Liang, T. Hao, C. Yin, X. Yang, H. Fu, X. Zheng, R. Li, D. Xiao, H. Chen, Eur. J. Inorg. Chem. 2017 (2017) 4149–4157, https://doi.org/10.1002/ejic.201700700.
[14] R. Esteghamat-Panah, H. Hadadzadeh, H. Farrokhpour, J. Simpson, A. Abdolmaleki, F. Abyar, Eur. J. Med. Chem. 127 (2017) 958–971, https://doi.org/10.1016/j.ejmech.2016.11.005.
[15] R.K. Gupta, G. Sharma, R. Pandey, A. Kumar, B. Koch, P.Z. Li, Q. Xu, D.S. Pandey, Inorg. Chem. 52 (2013) 13984–13996, https://doi.org/10.1021/ic401662d.
[16] K.M. Boyle, J.K. Barton, J. Am. Chem. Soc. 140 (2018) 5612–5624, https://doi.org/10.1021/jacs.8b02271.
[17] D.L. Ma, L.J. Liu, K.H. Leung, Y.T. Chen, H.J. Zhong, D.S. Chan, H.M. Wang, C. H. Leung, Angew. Chem. Int. Ed. 53 (2014) 9178–9182, https://doi.org/10.1002/anie.201404686.
[18] T.M. Khan, N.S. Gul, X. Lu, R. Kumar, M.I. Choudhary, H. Liang, Z.F. Chen, Dalton Trans. 48 (2019) 11469–11479, https://doi.org/10.1039/c9dt01951k.
[19] H.-Q. Zheng, Y.-P. Guo, M.-C. Yin, Y.-T. Fan, Chem. Phys. Lett. 653 (2016) 17–23, https://doi.org/10.1016/j.cplett.2016.04.064.
[20] R. Dheepika, R. Abhijnakrishna, P.M. Imran, S. Nagarajan, RSC Adv. 10 (2020) 13043–13049, https://doi.org/10.1039/d0ra00210k.
[21] S.B. Yadav, S.S. Sonvane, N. Sekar, Spectrochim. Acta A 224 (2020) 117421, https://doi.org/10.1016/j.saa.2019.117421.
[22] P. Garg, U. De, N. Dehury, H.S. Kim, S. Patra, J. Chem. Sci. 130 (2018), https://doi.org/10.1007/s12039-018-1492-6.
[23] Y.-Y. Lü, L.-H. Gao, M.-J. Han, K.-Z. Wang, Eur. J. Inorg. Chem. 2006 (2006) 430–436, https://doi.org/10.1002/ejic.200500748.
[24] H.G. Zhang, X.T. Tao, K.S. Chen, C.X. Yuan, S.N. Yan, M.H. Jiang, Chin. Chem. Lett. 22 (2011) 647–650, https://doi.org/10.1016/j.cclet.2010.12.005.
[25] F.X. Wang, M.H. Chen, X.Y. Hu, R.R. Ye, C.P. Tan, L.N. Ji, Z.W. Mao, Sci. Rep. 6 (2016) 38954, https://doi.org/10.1038/srep38954.
[26] J.J. Cao, Y. Zheng, X.W. Wu, C.P. Tan, M.H. Chen, N. Wu, L.N. Ji, Z.W. Mao, J. Med. Chem. 62 (2019) 3311–3322, https://doi.org/10.1021/acs.jmedchem.8b01704.
[27] R.R. Ye, C.P. Tan, L.N. Ji, Z.W. Mao, Dalton Trans. 45 (2016) 13042–13051, https://doi.org/10.1039/c6dt00601a.
[28] Y. Zheng, L. He, D.Y. Zhang, C.P. Tan, L.N. Ji, Z.W. Mao, Dalton Trans. 46 (2017) 11395–11407, https://doi.org/10.1039/c7dt02273e.
[29] Y. Li, C.P. Tan, W. Zhang, L. He, L.N. Ji, Z.W. Mao, Biomaterials. 39 (2015) 95–104, https://doi.org/10.1016/j.biomaterials.2014.10.070.
[30] T. Morimoto, H. Uno, H. Furuta, Angew. Chem. Int. Ed. 119 (2007) 3746–3749, https://doi.org/10.1002/ange.200604371.
[31] S. Wu, Y. Zhang, F. Ren, Y. Qin, J. Liu, J. Liu, Q. Wang, H. Zhang, Food Chem. 245 (2018) 613–619, https://doi.org/10.1016/j.foodchem.2017.10.122.
[32] W.X. Zong, J.D. Rabinowitz, E. Mol. Cell. 61 (2016) 667–676, https://doi.org/10.1016/j.molcel.2016.02.011.
[33] S. Pustylnikov, F. Costabile, S. Beghi, A. Facciabene, Transl. Res. 202 (2018) 35–51, https://doi.org/10.1016/j.trsl.2018.07.013.
[34] X. Zhang, S. Zhang, S. Zhu, S. Chen, J. Han, K. Gao, J.Z. Zeng, X. Yan, Anal. Chem. 86 (2014) 5232–5237, https://doi.org/10.1021/ac500918g.
[35] S. Vyas, E. Zaganjor, M.C. Haigis, Cell 166 (2016) 555–566, https://doi.org/10.1016/j.cell.2016.07.002.
[36] T. Nakajima, T. Yokota, Y. Shingu, A. Yamada, Y. Iba, K. Ujihira, S. Wakasa, T. Ooka, S. Takada, R. Shirakawa, T. Katayama, T. Furihata, A. Fukushima, R. Matsuoka, H. Nishihara, F. Dela, K. Nakanishi, Y. Matsui, S. Kinugawa, Sci. Rep. 9 (2019) 3535, https://doi.org/10.1038/s41598-019-40419-7.
[37] S. Fulda, L. Galluzzi, G. Kroemer, Nat. Rev. Drug Discov. 9 (2010) 447–464, https://doi.org/10.1038/nrd3137.
[38] S.S. Sabharwal, P.T. Schumacker, Nat. Rev. Cancer 14 (2014) 709–721, https://doi.org/10.1038/nrc3803.
[39] M.I. Khan, A. Mohammad, G. Patil, S.A. Naqvi, L.K. Chauhan, I. Ahmad, Biomaterials 33 (2012) 1477–1488, https://doi.org/10.1016/j.biomaterials.2011.10.080.
[40] H. Vakifahmetoglu-Norberg, A.T. Ouchida, E. Norberg, Biochem. Bioph. Res. Co. 482 (2017) 426–431, https://doi.org/10.1016/j.bbrc.2016.11.088.
[41] A. Gross, Biochim. Biophys. Acta 1857 (2016) 1243–1246, https://doi.org/10.1016/j.bbabio.2016.01.017.
[42] A.S. Don, P.J. Hogg, Trends Mol. Med. 10 (2004) 372–378, https://doi.org/10.1016/j.molmed.2004.06.005.
[43] Y. Zheng, D.Y. Zhang, H. Zhang, J.J. Cao, C.P. Tan, L.N. Ji, Z.W. Mao, Chem.Eur. J. 24 (2018) 18971–18980, https://doi.org/10.1002/chem.201803630.
[44] R.-R. Ye, Z.-F. Ke, C.-P. Tan, L. He, L.-N. Ji, Z.-W. Mao, Chem.Eur. J. 19 (2013) 10160–10169, https://doi.org/10.1002/chem.201300814.
[45] M. Zhang, J. Zheng, R. Nussinov, B. Ma, Sci. Rep. 7 (2017) 2635, https://doi.org/10.1038/s41598-017-02825-7.
[46] J.H. Bae, J.-W. Park, T.K. Kwon, Biochem. Bioph. Res. Co. 303 (2003) 1073–1079, https://doi.org/10.1016/s0006-291x(03)00479-0.
[47] J.C. Martinou, R.J. Youle, Dev. Cell 21 (2011) 92–101, https://doi.org/10.1016/j.devcel.2011.06.017.